Renewable Energy 222 (2024) 119929

Contents lists available at ScienceDirect

Renewable Energy

journal homepage: www.elsevier.com/locate/renene

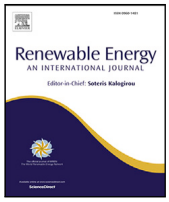

Modelling and analysis of the horizontal configuration of tidal fences in barrages

M.C. Verbeek [a,*], H. Talstra [b], R.J. Labeur [a], W.S.J. Uijttewaal [a]

[a] Department of Hydraulic Engineering, Delft University of Technology, Stevinweg 1, Delft, 2628 CN, The Netherlands
[b] Svasek Hydraulics, Schiehaven 13G, Rotterdam, 3024 EC, The Netherlands

ARTICLE INFO

Keywords:
Tidal fences
Sub-grid calculation
Tidal basin hydrodynamics
Tidal barrage
Modelling

ABSTRACT

Tidal stream turbines are becoming an affordable option for harvesting sustainable energy in coastal areas. They can be retrofitted in barrages, providing an integral solution for flood protection and emission-free power generation, within environmental constraints. To optimize the turbine-barrage configuration with respect to these objectives, simulation tools are needed to predict the efficiency of the turbines as well as their impact on the adjacent tidal system. These tools should be based on an accurate representation of the underlying flow processes, which cover a wide range of spatial scales — from meters at the barrage and turbines to tenths of kilometers in the tidal basin. This article presents the development of such a tool by linking an analytical model for turbine fences in barrage gates to a regional flow model. The turbine model is validated with experimental data, and data from a thoroughly monitored tidal energy pilot project. Simulations reveal how clustering the turbines in small arrays can increase their efficiency, owing to array blockage effects, with only little effect on the tidal exchange. We also demonstrate the potential of using turbine fences to manipulate the tidal jet, issued from the barrage, with benefits for coastal — and wildlife protection in the basin. The presented research helps understanding how turbine fences in barrages can be configured with high energy yield and calculated impact to the environment.

1. Introduction

The EU targets to further decarbonize the energy system, as this is critical to reach climate objectives in 2030 and 2050 [1]. Tidal stream turbines, which are a promising technology in a development stage, are becoming an affordable option for sustainable energy harvesting in coastal areas, and, in this way, contribute to this target [2]. Besides, the EU aims to conserve its natural capital and protect its citizens from environment-related hazards, such as coastal floods. However, these objectives are complex and interlinked, which makes it non-trivial to develop and optimize tidal energy projects in practice. In the research described in this paper we set up a modelling tool specifically for this purpose and apply it to an existing pilot project to shed light on the possible trade-offs and compromises of the above objectives.

In the tidal energy pilot under consideration (in the Eastern Scheldt tidal basin, The Netherlands) the above objectives could actually be combined. Five horizontal-axis tidal turbines (a fence) were retrofitted in a single gate of an open storm surge barrier or tidal barrage, in order to harvest sustainable energy from the passing tidal current. Hereby, the flood protection function and estuary ecosystem value were warranted over the span of the pilot, between 2015 and 2019 (and later between 2021 and 2023) [3–5]. In order to understand how energy yield as well as flood protection within environmental constraints can still be served simultaneously while retrofitting more turbine fences in neighbouring gates of a barrage, a modelling tool is needed that can predict turbine power production as well as the impact of the barrage and turbines on the adjacent tidal system. By incorporating the main physical processes, such a tool should also be instrumental in applying lessons learned to other tidal sites.

Specifically, the desired tool must be able to predict how small-scale flow processes associated with the turbines affect larger-scale flow processes in a tidal basin, and vice versa (see Figs. 1 and 2). At small scales, an individual turbine device influences the blockage of its neighbour turbine through bypass flow and wakes [6,7]. Besides, the flow through the barrage itself also interacts with the turbine [4]. At larger scales, the distribution and amplitude of the tidal current over the barrage is affected by the sum of these processes, and vice versa. In turn, these large-scale processes have impact on e.g. discharge distribution and sediment transport [3], which are important to flood-

* Corresponding author.
E-mail addresses: verbeek.m.tud@gmail.com (M.C. Verbeek), talstra@svasek.com (H. Talstra), r.j.labeur@tudelft.nl (R.J. Labeur), w.s.j.uijttewaal@tudelft.nl (W.S.J. Uijttewaal).

https://doi.org/10.1016/j.renene.2023.119929
Received 12 December 2022; Received in revised form 6 December 2023; Accepted 29 December 2023
Available online 2 January 2024

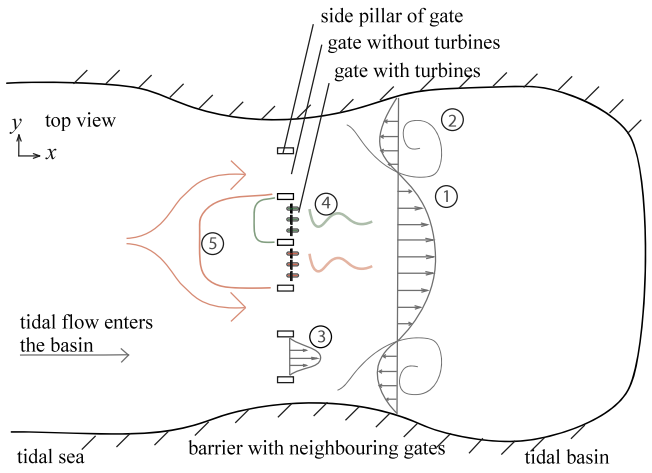

Fig. 1. Schematic overview (top) of turbine-barrage flow interaction at the basin scale, of $\mathcal{O}$(1-10) km, illustrating the relevant processes: 1. flow contraction in the tidal channel, 2. large-scale turbulence structures, 3. flow contraction in barrage gates, 4. turbine added resistance, 5. turbine-turbine and gate-gate interactions.

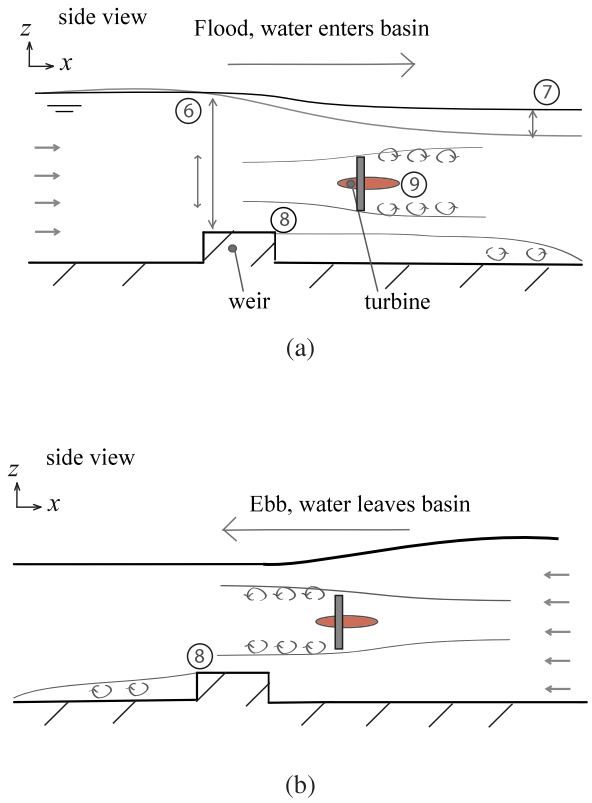

Fig. 2. Schematic overview (side) of turbine-barrage flow interaction at device scale, of $\mathcal{O}$(1-10) m, during flood flow (a) and ebb flow (b), illustrating the relevant processes: 6. flow contraction by local blockage, 7. free-surface level variation, 8. flow expansion downstream of the weir, 9. flow expansion in the turbine wake.

and nature protection of a basin. Due to this interaction of scales, an important requirement of the desired tool is the dynamic coupling of flow phenomena at both scale levels: from flow patterns at the scale of a single turbine device, of $\mathcal{O}$(1-10) m, up to flow patterns at the scale of a barrage and the wider tidal basin, of $\mathcal{O}$(1-10) km.

The described coupling of scales usually comes at the cost of an increased computational effort. Obviously, it is desirable to minimize this effort where possible. This can be achieved in two ways. Firstly, by modelling small-scale turbine processes (such as the flow through and bypassing a turbine device) in a sub-grid manner, using a parameterization which accounts for the relevant physical processes, and coupling this to a larger-scale numerical flow model. And secondly, by applying local mesh refinement in the larger scale model near the barrage and turbine fence (to accurately and efficiently resolve the coupling of scales), while using a coarser mesh resolution in the far field. In this study, this is achieved by employing an unstructured triangular mesh combined with a numerical flow model based on the finite element method.

There are different ways to include sub-grid flow effects of tidal stream turbines or barrages in a regional (numerical) flow model. A first type employs a modified (mass) flux at the position of the turbine [8] or barrage [9] location, using a line discontinuity in the mesh. A second type uses a mesh-interpolated momentum sink representative of the force applied by the turbine to the flow (e.g. [10]). The first approach has the advantage that discontinuities in the discrete flow velocity and water level associated with the turbine(s) are automatically captured by the mesh. This avoids a numerical boundary layer (wiggles) that would otherwise occur if the local mesh resolution is too coarse with respect to the horizontal extent of the disturbed flow field. This layer can then only be suppressed by increasing the viscosity which also obscures, however, the turbine-gate interaction.

With this in mind, the aim of the research described in this paper is twofold. Firstly, to establish the elementary dynamics of a single turbine-gate configuration, in order to develop and validate an efficient sub-grid parameterization which describes the energy yield and head-discharge relation of a turbine fence mounted in a barrage with gates. Secondly, to couple this sub-grid parameterization, using internal boundaries, with a larger-scale numerical flow model and applying it to a tidal power pilot project in order to assess the effects of alternative turbine configurations on energy yield, discharge distribution, tidal prism, and system functions related to natural capital and coastal protection. The findings will help understanding how to optimally combine complex EU ambitions on coastal protection and energy generation within environmental constraints in a tidal energy project.

This approach has a few innovative aspects. First, a physics-based sub-grid model is developed for the specific case of turbine fences in barrage gates. The latter increase the turbine thrust, as the flow is strongly contracted, which requires an extension of existing models, e.g. [11], with a barrage weir. Second, while hardly used in literature, the implementation of the sub-grid model by means of internal boundaries is exploited to resolve the local flow details that drive the turbine-gate interaction — which is all important here. Third, and last, the resulting flow field and turbine power are validated using field and laboratory data from a turbine fence in a barrage. The availability of data from commercial-scale operating turbines in representative environments is unique and the combination of a turbine with a weir has not been studied in the field nor in a laboratory setting before.

In view of the aims above, this paper is structured as follows. Section 2 describes the developed sub-grid turbine-weir parameterization, as well as its coupling with a larger-scale numerical model solving the two-dimensional (2D) shallow water equations. The resulting modelling tool is validated using (successively) field data and experimental data of turbines in hydraulic structures [4,5]. In Section 3, this tool is applied to the above mentioned pilot project in the Eastern Scheldt storm surge barrier (barrage). Site-specific as well as general results are presented in Section 3.4. The discussion in Section 4 integrates findings from both parts of the scope: the applicability range of the developed sub-grid tool, and the ensuing design considerations for tidal energy sites. Besides, some trade-offs and compromises between the various (complex and interlinked) design objectives are considered. Conclusions are formulated in Section 5.

2. Sub-grid turbine model and its coupling to larger scales

This section describes the development of the sub-grid turbine model and its coupling to a larger-scale model for computing tidal flows. To this end, we will first identify the physical processes relevant to each scale in Section 2.1. Concerning the turbines, we next derive a theoretical formulation aggregating the elementary dynamics of a turbine fence mounted in a barrage gate with a weir (Section 2.2.2). For an individual turbine, this provides a relation between the local discharge, the head difference over the turbine and the power production. The resulting parameterization is implemented in a tidal flow model, using interior boundary conditions, thereby achieving the desired coupling of scales. The overall approach is validated in Section 2.3.

2.1. Governing physical processes

We consider a semi-enclosed tidal basin, having a open barrage in its inlet; see Fig. 1 for a conceptual lay-out of the system. Here, a tidal inlet refers to the sea body between two islands or headlands, where the tidal exchange flow locally contracts. In this work, the barrier (or barrage) consists of parallel gates, spanning the width of the tidal inlet. Each of the gates is in fact a small channel formed by side pillars and a bottom beam (weir). In the gate an array of tidal turbines can be installed, see Fig. 2. An array (often referred to as a fence) consists of tidal devices placed next to each other, perpendicular to the flow. The performance and impact of these arrays of turbines are the result of a superposition of processes. Next, we introduce them in order of their associated length scale, which is roughly 1–10 km for the channels (horizontal length or width), and typically 1–10 m for the gates and devices (diameter of the turbine blade swept area).

2.1.1. Channel scale

Fig. 1 distinguishes five channel-scale processes, which need to be resolved with sufficient detail when when using a numerical flow model for turbine-barrage interaction. With reference to the figure, these processes are discussed briefly below.

The tidal flow towards the barrage (1) contracts in the tidal inlet. In [12] it was shown that this process is associated with large horizontal gradients of the flow velocity, and can be typified as a (tidal) jet. The flow further contracts (3) within the barrage gate (horizontally) and over the weir (vertically). The corresponding acceleration of the flow velocity enhances turbine thrust and power coefficients, mainly as a result of an additional pressure difference over the turbines [6,13]. The subsequent expansion of the flow behind the barrage (2) leads to large-scale, quasi-horizontal turbulence driving large gyres along the side slopes of the inlet channels.

The turbines themselves decelerate the flow locally through their so-called added resistance (4), as energy head of the flow is lost in turbine power extraction and energy dissipation in the turbulent wakes [13]. As a result of this resistance, single turbine devices and arrays of turbine fences interact with each other (5) through water level set-up and bypass flows. In [7,14] it was postulated that there exists an optimal intra-turbine spacing (referred to as local blockage) and inter-array spacing (array blockage) maximizing the power coefficient of a single turbine. The power extraction of the tidal farm as a whole can therefore be optimized by altering the intra-turbine and intra-array spacing, depending on the total number of devices (global blockage). The optimum strikes a balance between the higher efficiency of a single device, when operated in clusters of devices, and the added resistance of the overall farm to the flow, in conjunction with the response of the adjacent tidal basin (basin efficiency).

2.1.2. Gate-turbine scale

Fig. 2 illustrates four device-scale processes, which will be included in a sub-grid model and coupled to the aforementioned large-scale flow model. With reference to the figure these processes are discussed below.

In a free, unbounded flow, a turbine can capture at most a fraction of 16/27 of the incoming energy flux through a plane with the same size as the rotor swept area. This famous result was derived analytically by Betz [15], and is due to the flow bypassing the turbine because of the higher local resistance. In a constrained flow however, such as in the barrier gate (6), the bypass flow is suppressed leading to a higher limit of power extraction. This effect is governed by the local blockage B (or occupation ratio) of the turbine, which is defined as the ratio of the streamwise projection of the rotor swept area and the channel cross section. It was shown in [11] that the limit of power extraction increases with a factor of $(1-B)^{-2}$. In a similar way, spatial and temporal variations of the free surface level (7) influence the power extraction, by altering the local blockage, an effect that is characterized by the local Froude number [16].

Turbine performance is furthermore dependent on the local flow patterns and the pressure field within the gate. In particular, these are affected by the crest of the weir (8). The weir causes an additional contraction of the flow, which also involves a negative pressure gradient. Moreover, the recirculation zone behind the weir (9) interacts with the wake flow of the turbine, slowing down its recovery. All this will further enhance the performance of the turbine, depending also on the position of the turbine with respect to the weir. In [4] an analytical model was postulated and validated, accounting for the effects of the weir on the turbine performance and added resistance.

2.2. Modelling approach

The channel-scale processes (1-5) are basically governed by the two-dimensional shallow water equations (SWE) where the equations of motion of the flow are averaged over the depth [17]. This averaging relies on the pressure being hydrostatic in the vertical direction, which is obviously not the case around the gates and turbines. Therefore, the small-scale processes (6-9) have to be taken into account by means of a sub-grid model, treating the non-hydrostatic effects in a semi-analytical manner. In our approach, we express the discharge through a gate – with or without turbines – in terms of the head difference over the gate and the device properties. The resulting discharge relation will be coupled to the large-scale model by means of an interior boundary condition. Details of the approach are described below.

2.2.1. Shallow-water flow model

The shallow water equations that govern the channel-scale flow are discretized using a finite element method based on a numerical approach that was introduced in [18] and further developed in [19,20], see also [21,22] (see equations in Appendix B). The method employs a computational mesh consisting of triangles, that can have arbitrary size and shape, which conveniently accommodates to irregular geometries and allows for a flexible local mesh refinement in the domain of interest.

Importantly, near the barrage a sufficient mesh resolution is required in order to warrant a correct reproduction of the intra-turbine and inter-array interactions. Also the wakes from arrays of turbines and the adjoining lateral recirculation zones need to be resolved with sufficient detail (combined with a horizontal turbulence model) in order to predict the overall efficiency of the tidal farm correctly. A maximum triangle size of $\mathcal{O}(10)$ m (turbine spacing) is considered necessary here, which can be furnished by refining the triangles locally, keeping the total number of triangles in the mesh acceptable for computational efficiency.

Along the exterior boundaries of the model domain, either the water level or the flow velocity must be prescribed. The actual boundary

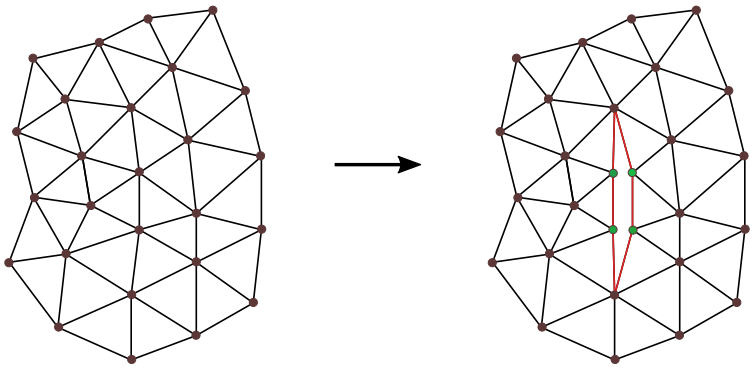

Fig. 3. Creation of an interior boundary (indicated red) by duplication of associated nodes (indicated green).

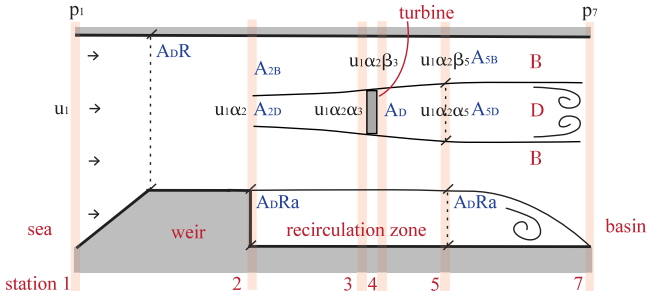

Fig. 4. A schematic sketch of the flow passing a barrage weir and turbine via a streamtube passing the turbine (indicated D), a bypass streamtube (indicated B), and a recirculation zone of the weir, driven by a pressure difference ($p_7 - p_1$). The numbers refer to the stations of the model schematization. The respective velocities within the domain are expressed as a factor times the inflow velocity u_1 (at station 1), using the velocity factors α in the turbine streamtube and β in the bypass. The cross-sectional area of a streamtube at each station is expressed as the product of the rotor-swept area A_D, the relative weir area a, and the blockage $1/R$. An overview of the velocity and cross section of each streamtube is provided in the supplementary material [23].

conditions to be imposed depend on the situation at hand which, for our case, will be specified in Section 3.2.

In addition, we introduce interior boundaries in order to implement the sub-grid turbine model. These boundaries are located at and aligned with the barrage gates and turbines, and are created by locally disconnecting the mesh, see Fig. 3. The action of the turbines and/or barrage gates is simulated by expressing the volume flux between the resulting pairs of opposite points in terms of the water level difference between these points. The corresponding head-discharge relation is used to prescribe the flow velocity at interior boundaries, which provides the desired dynamic coupling between water levels at neighbouring nodes on both sides of the barrage location. It now remains to quantify this relation for the various gate-turbine configurations.

2.2.2. Sub-grid turbine model

The basis of the head-discharge relation used for the sub-grid turbine parameterization is the analytical model given in [4] (see Fig. 4). In this model, the device-scale processes are quantified by combining two existing approaches, a head-discharge relation describing the flow over a long-crested weir [17], and an actuator disk model to calculate the performance of a single turbine in a channel [11]. The model aims to account for the influence of a weir (or other abrupt expansion of the flow) on the turbine performance and resistance in a single gate of a barrage, which distinguishes it from the schematized model in [11]. The resulting head-discharge relation for the turbines/gates takes the following generic form,

$$q = d_c u_c = \left(\zeta - b_c\right)\sqrt{\frac{2g\,\Delta h}{f}} \tag{1}$$

in which q is the volume flux at the gate per unit width, $d_c = \zeta - b_c$ ($= A_D R$ in Fig. 4) is the water depth at the weir crest, ζ and b_c are, respectively, the water level and bed level at the weir crest, $u_c (= u_1\alpha_2$ in Fig. 4) is the depth-averaged flow velocity at the crest, g is the gravitational constant, Δh ($= (p7 - p1)/(\rho g)$ in Fig. 4) is the head difference over the gate, and f is a dimensionless head loss coefficient.

The geometrical parameters ζ and b_c depend directly on the dimensions of the gate and the adjoining water level. To account for the influence of the free surface height on the blockage, we use a time-variable, uniform water level ζ by averaging the water levels upstream and downstream of the gate obtained from the shallow-water model. This is allowed if the head difference Δh is small relative to the water depth, and only acts as a pressure force driving the flow.

The discharge coefficient f emulates all device-scale processes, and depends on the specific turbine-weir configuration (one example of turbine downstream a weir is given in Fig. 4). We distinguish turbines on a flat bed, turbines upstream of a weir, turbines downstream of a weir, and a weir only. The different cases are characterized by the distance between the turbine rotor and weir crest, crest height a, the rotor diameter (blockage $\frac{1}{R}$), and the deceleration of the flow velocity behind the turbine α_5, (all variables are seen in Fig. 4). The latter is specified as the dimensionless ratio of the initial velocity in the turbine wake and the undisturbed ambient velocity. This parameter α_5 depends on the turbine operation and is to be obtained from experiments and field tests.

To derive closed algebraic expressions for f, the flow passing the weir and turbines is schematized by means of two streamtubes, a streamtube passing the rotor disk, and a streamtube following the entire bypass flow (see Fig. A.12). Assuming quasi-steady flow (inertia terms and local mass storage can be neglected), one-dimensional balances of mass, momentum and energy apply to both streamtubes. The tubes interact via pressure forces, that depend on their spatial configuration, leading to a set of coupled equations. This can be solved analytically to give the distribution of the flow over both streamtubes, the head-loss coefficient f, and the turbine thrust and power coefficients. This important information regarding the sub-grid parameterization is included in Appendix A and the supporting material [23], as the resulting algebra is lengthy.

The derived head-discharge relation is applied to the flow component normal to the interior boundary. This is in accordance with the physics of turbines, as horizontal-axis turbines extract streamwise momentum from the flow. However, it also requires that the mesh contours within the model are aligned with the turbine-swept planes, which is easily accomplished when using an unstructured mesh. Provided this condition is met, our sub-grid turbine parameterization can be coupled to other types of spatial discretization as well, for which computer source code is available in the supporting material [23].

2.3. Model validation

The coupled model has been validated elaborately with field — and experimental data, which is described in detail in the supporting material [23]. In essence, the validation showed that the model predicts the magnitudes of the head loss and discharge through a gate with turbines quite well, with a relative accuracy of more than 80%, which is close to the accuracy of the measurements. Furthermore, the model very accurately predicts the turbine thrust and power coefficients. However, for a turbine placed upstream of a weir (ebb situation) the power was overestimated by approximately 60% in the field situation. With a view to the results below, the latter implies that for this particular turbine-weir configuration the computed added resistance of the tidal farm may be on the conservative side. This overestimation for the ebb phase has three main causes: (1) the decelerating effect of the turbine strut (situated in front of the rotor swept plane during ebb) which is not incorporated in the model, (2) the overestimation of the near-field wake expansion, and (3) the overestimation of the blockage factor (which is well-defined only for the flood situation with the turbine downstream of the barrage).

There remain a few points of attention when applying the coupled model. First, the wake recovery downstream of the turbine arrays (mid field) and the barrage (far field) influences the performance of the tidal farm . This is simulated by using a Smagorinsky turbulence closure model [24], an approach that should be refined however if wake development in the mid - and far field need to be resolved with greater accuracy. Furthermore, the bed level used in the mesh at the sub-grid location must be based on the nearby bottom bathymetry, excluding the weir-gate geometry, as the later is already accounted for in the sub-grid model. Lastly, the wake velocity factor α_5 is used as a calibration parameter for which the turbine characteristics must be known beforehand in order to predetermine a realistic range of values (see Section 3.2.2 for the calibration of α_5).

3. Case study eastern scheldt tidal basin

This section describes how the developed tool is used in a case study. We determine an optimal configuration of turbines in the storm surge barrier of the Eastern Scheldt by varying the number of turbines and their spacing. First, the study area and the tidal energy pilot project are introduced after which the tidal model for the Eastern Scheldt and the sub-grid model for the adopted turbines are calibrated. Thereafter, the results of the optimization study are analysed, considering the performance as well as the environmental impact of the tidal farm.

3.1. Tidal dynamics

The Eastern Scheldt is a tidal basin located in the southern part of the North Sea, with a large semi-open storm surge barrier in its inlet (see Fig. 5). The barrage has a total length of 8 km, spanning the three tidal channels (from North to South) Schaar, Hammen and Roompot, and also includes two barrier islands separating the channels. The construction of the barrage consists of a submarine dam, with sixty-two parallel open gates on top distributed evenly over the three channels. The gates, which are 40 m in width, are formed by concrete piers with a bed beam - or weir. Bed protection, consisting of boulders, extends to six hundred meters up- and downstream of the barrage to protect the local seabed against the impact of the high current velocities near the barrage.

A pilot project that started in 2015, involved the deployment of five horizontal-axis tidal turbines which were retrofitted in one gate of this barrage to harness energy from the passing tidal current [3–5]. The flow velocity inside the barrage gates amounts up to 5 ms^{-1}, which makes this form of energy generation attractive at this location. Interestingly, the storm surge barrier has room for retrofitting many more turbines. However, it is unclear how the different functions of the barrage structure are warranted when up-scaling the energy yield. The two most important conditions are discussed below and reflected upon in the results.

The storm surge barrier's main objective is flood protection. In particular, the gates of the dam can be closed to protect the south-western part of the Netherlands from coastal flooding. For the integrity of this structure it is imperative that the scour holes, which are forming at either side of the barrage by the strongly contracting flow at the tidal inlet [25], are not further deepened. In [12] a mitigation strategy for this erosion was proposed where the lateral non-uniformity of the flow upstream of the scour hole is reduced. Interestingly, this is what the tidal turbines could possibly realize, when positioned in the centre of the tidal jet.

Another objective of the barrage is to preserve the nature capital of the Eastern Scheldt basin. The barrage is left partly open to allow tides to pass, thereby sustaining the ecosystem of the area. The sandy inter-tidal flats, which are the most biodiverse locations of the area, need sufficient sediment supply by the tide. Hence, an optimal configuration of turbines involves a minimal reduction of the tidal volume (discharge) and maintains a maximal tidal asymmetry. This is crucial as the construction of the open barrage itself already lowered the so-called tidal volume by 30 percent [26]. Hence, an optimal turbine configuration in terms of energy yield can compromise the ecological objectives of a site, and vice versa.

3.2. Model set-up and calibration

This section summarizes the main issues of the application and calibration of the coupled model to the Eastern Scheldt case study. An extensive overview and discussion of the calibration and the resulting model settings is given in the supporting material [23].

3.2.1. Shallow-water flow model

The shallow-water flow model encompasses the Eastern - and Western Scheldt tidal basins, and the adjacent part of the North Sea (Fig. 6). The size of the triangular elements roughly varies from 5 m at the barrage, via 50 m at the edge of the bed protection and 100 m in the tidal basin, to 2 km in the far field at open sea, which results in about 340,000 elements. The bathymetry is based on data sets of Rijkswaterstaat (Dutch Ministry of Infrastructure), with a high level of detail near the barrage (Fig. 7). The tidal water level is prescribed along the seaward boundary of the model, using 95 harmonic constituents obtained from a continental shelf model [27].

The model has been calibrated in [27] in terms of water levels and discharges; the former using fixed gauges across the region, the latter using Acoustic Doppler Current Profiler (ADCP) transects sailed with a ship (observed velocities have been integrated over various cross sections within the basin to obtain the discharges in the tidal channels, see Fig. 7a). As an example, Fig. 7b demonstrates the correspondence between the observed and computed discharge in the Roompot inlet (transect no. I).

3.2.2. Sub-grid turbine model

At the barrage, interior boundaries are used in combination with the sub-grid turbine model, in such a way that many different configurations of gates with or without turbines can be chosen. The pillars of the storm surge barrier have been included in this boundary by accounting for their respective blockage widths, which amounts to 12% of the total barrage width.

The velocity coefficient α_5 in the turbine model is calibrated using field data from the pilot project at the Eastern Scheldt barrier [4]. Based on in-situ velocity measurements along the wake centreline of one of the installed turbines, a velocity coefficient of 0.65 was derived, which conforms to the range of values (0.56 - 0.95) found in experiments [4]. However, this result relies on the velocity profile that was adopted to relate the measured velocity in the wake centreline to an average value

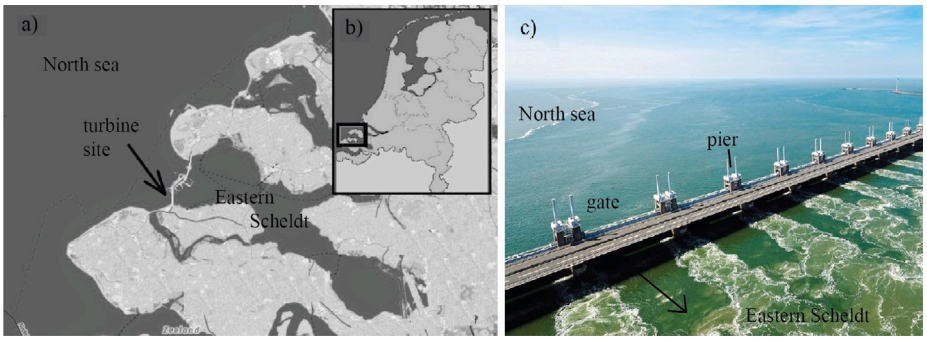

Fig. 5. The Eastern Scheldt estuary; horizontal planform showing turbine site (a), location in the Netherlands (b), aerial photograph of the storm surge barrier (barrage) and its gates.
Source: Rijkswaterstaat.

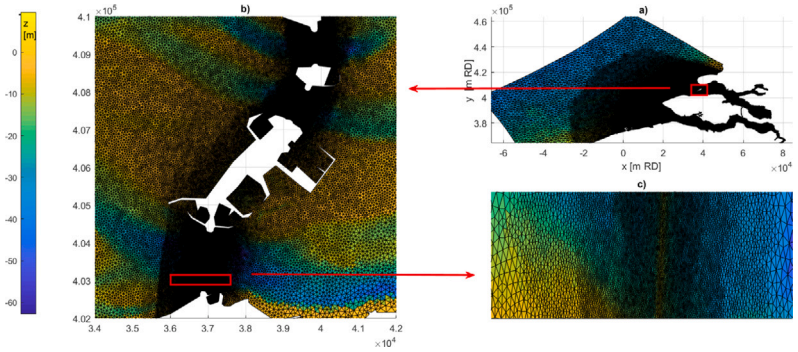

Fig. 6. Spatial discretization shallow-water flow model, colorbar indicates depth [m] with respect to mean sea level; overall mesh including Eastern Scheldt, Western Scheldt and adjacent North Sea (a), mesh refinement at the barrage (b); mesh refinement near the gates (c).

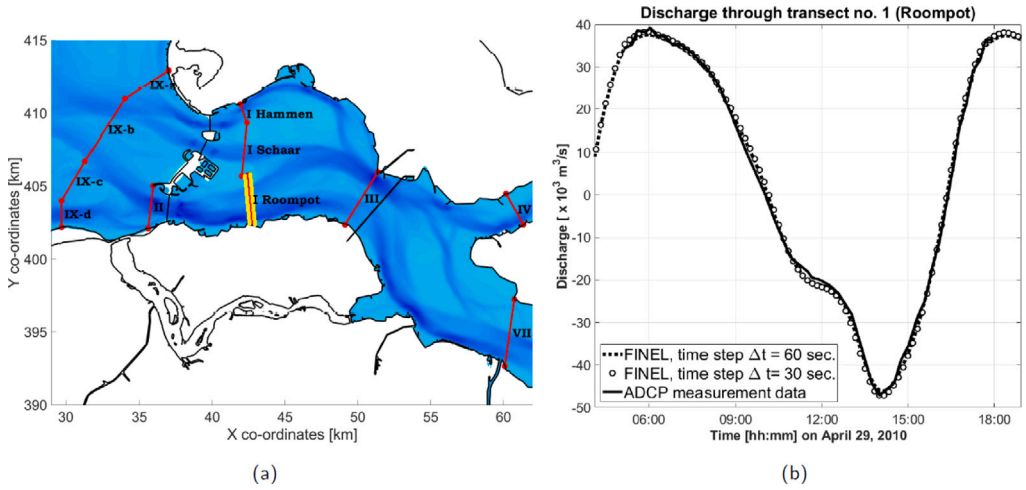

Fig. 7. Calibration of shallow-water flow model; locations of ADCP transects across the Eastern Scheldt basin used for model calibration (a), computed and observed discharge past transect no. I in the Roompot inlet (marked in yellow). (b).

characterizing the entire turbine wake streamtube.[1] We therefore perform a sensitivity analysis by applying the coupled model to the pilot project, for a full neap-spring tidal cycle, using values for α_5 between 0.55 and 0.75. A sensitivity analysis of the performance coefficients C_P and C_T for a range of α_5 values for the different cases specified by f is provided in Fig. 4 of the supplementary material [23].

Fig. 8 shows computed and measured thrust, power and velocity data versus the water level difference over the barrage. For the considered range of α_5, the computed turbine power and thrust are almost similar, but the computed local velocity at the turbine shows a better agreement for a velocity factor of 0.65, confirming the value proposed in [4], and which is adopted here. At the same time, the computed thrust and power agree well with the measured values during the flood phase, while during ebb these are overestimated by approximately 60%. In line with the observations, the computed added resistance of the turbines is larger during ebb (turbine upstream of the weir) than during flood (turbines downstream of the weir), where the latter is also slightly underestimated in the computations.

[1] The measured velocity deficit in the wake centreline equals half the undisturbed incoming flow velocity which, by assuming a parabolic velocity profile over the wake cross section, corresponds to an average velocity factor of 0.65 for the wake streamtube.

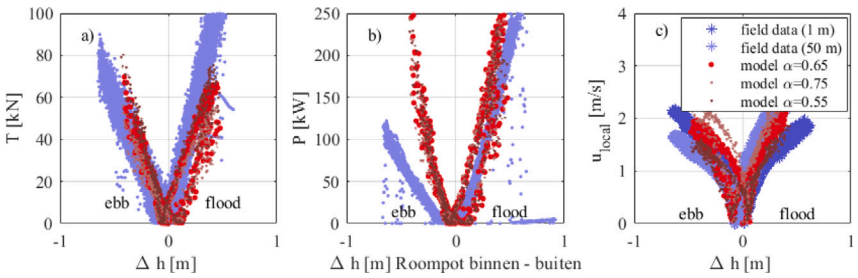

Fig. 8. Calibration of the sub-grid turbine model; turbine thrust (a), turbine power (b), and flow velocity at turbine (c) versus corresponding water level difference (Δh) over the barrage.

Finally, it should be noticed that the adopted value for α_5 is not necessarily the optimal value regarding power extraction, rather it is a value that corresponds to the observed turbine performance parameters and that we wish to reproduce here.

3.3. Scenarios

The trade-off between lowering the tidal volume (discharge) through the structure and increasing energy yield is studied by varying the turbine configurations in a systematic way. As a guiding principle we use the concept of multi-scale dynamics introduced in [6]. Turbine configurations are thus characterized in terms of their local blockage, array blockage and global blockage, relating the respective areas of obstruction to the total flow cross section for a turbine or group(s) of turbines [7]. The local blockage (B_L) is defined as,

$$B_L = \frac{\frac{1}{4}\pi D^2}{d\left(D + s_L\right)} \tag{2}$$

where D is the turbine diameter, d is the water depth and s_L is the intra-turbine spacing. Referring to a cluster of turbines in a single gate as an array, the array blockage (B_A) is defined as,

$$B_A = \frac{m\left(D + s_L\right)}{m\left(D + s_L\right) + s_A} \tag{3}$$

where m is the number turbines in a gate, and s_A is the horizontal distance between gates with turbines. In a similar way, the global blockage (B_F) is defined as,

$$B_F = \frac{n\left(m\left(D + s_L\right) + s_A\right)}{W} \tag{4}$$

where n is the number of gates with turbines and W is the total width of the barrage or inlet.

Our scenarios consider the southernmost inlet of the basin (Roompot) which has 31 gates spanning a total width of 1.5 km. Corresponding to the situation of the pilot study, the number of turbines in a gate (m) is set to 5, giving a local blockage B_L of 0.3. In order to generate independent combinations of farm - and array blockage, we vary the total number of gates with turbines (n), and the number of open gates alternately left open (s). This results in scenarios with 0, 1, 2, 5, 8, 10, 15 and 30 gates with turbines, where – starting at the 8th gate from the south (the location of the test station) – turbines are placed in neighbouring gates ($s_n = 0$), in every 2nd gate ($s_n = 1$), or in every 3rd gate ($s_n = 2$). The resulting combinations of global - and array blockage are summarized in Table 1.

In the simulations, overall discharge (tidal volume), power output and power coefficient of the turbines are monitored, while keeping the overall tidal forcing (mean neap-spring tidal cycle) and turbine performance parameters constant.

Table 1
Cross-table indicating the different model scenarios, varying the number of gates filled with turbines (n, global blockage B_F) and the number of gates left empty in between (s, array blockage B_A); number of turbines per gate (m) equals 5 (local blockage $B_L = 0.3$).

n	0	1	2	5	8	10	15	30
B_F	0	0.03	0.05	0.13	0.21	0.27	0.4	0.8
$s_n = 0,\ B_A = 1$	✓	✓	✓	✓	✓	✓	✓	✓
$s_n = 1,\ B_A = 0.5$		✓	✓	✓	✓	✓	✓	
$s_n = 2,\ B_A = 0.3$		✓	✓	✓	✓	✓		

3.4. Results

This section presents the modelling results of the considered scenarios. First, the general characteristics of the ambient tidal flow in the inlets of the Eastern Scheldt are described. Thereafter, the power output from the turbines and the ways in which turbines affect the tidal exchange are considered.

3.4.1. Reference scenario

For the reference scenario ($n = 0$), the flow towards the barrage contracts horizontally and vertically due to, respectively, the horizontal planform of the tidal inlets of the Eastern Scheldt and the presence of a bottom sill at the barrage [12]. This is illustrated in Fig. 9, showing computed flow fields in the inlet during the maximum ebb and flood stages. In every inlet a tidal jet forms that varies periodically in time in response to the tide, with a pronounced asymmetry between ebb and flood as described in [28]. A free shear layer with two counter rotating vortices is developing on either side of the jet directly downstream of the barrage. Paradoxically, the velocity in the jet increases in downstream direction, where also the depth increases due to the presence of scour holes. This effect is due to further contraction of the jet by the downward bed slope, a phenomenon that causes ongoing erosion of the scour holes [12]. Superimposed on the tidal jet, narrow neighbouring jets are present in the flow pattern, associated with the individual barrage gates. This general flow pattern confirms the schematization of the flow and the associated processes as outlined in Section 2.1.

3.4.2. Turbine scenarios: tidal discharge and power output

The results for the considered scenarios are summarized in Fig. 10, in terms of the tidal volume passing the tidal inlets, the power delivered by the turbines, and the associated power coefficient, which are plotted versus the global blockage (B_F).

For an increasing global blockage, the tidal volume passing the Roompot inlet initially decreases until a certain minimum — depending on the array blockage the reduction amounts upto 1.5% of the reference volume (Fig. 10a). This tidal reduction results from the additional resistance by the turbines, which increases with the total turbine area and also depends on the array spacing. Remarkably, the tidal volume partly recovers when turbines are distributed evenly over the full span of the barrage, instead of being placed in the mid sections only. The former is the case for low global blockage with high inter-array spacing, as well as for higher global blockage with lower inter-array spacing,

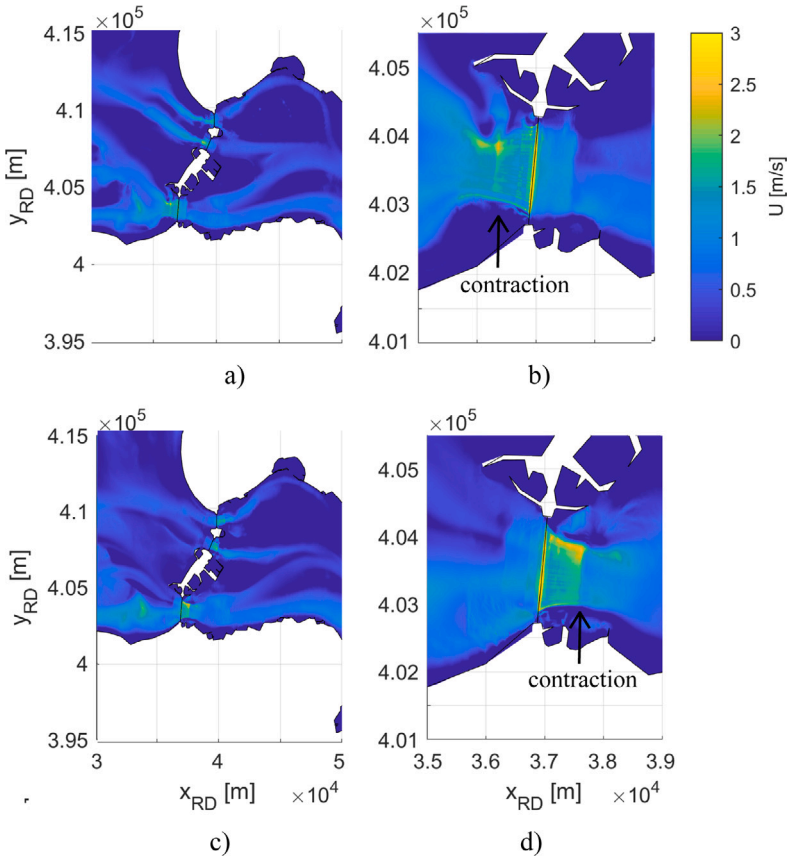

Fig. 9. Computed flow fields at the inlet of the Eastern Scheldt; western basin, maximum ebb (a), Roompot, maximum ebb (b), western basin, maximum flood (c), Roompot, maximum flood (d); colorbar indicates the depth-mean flow velocity magnitude.

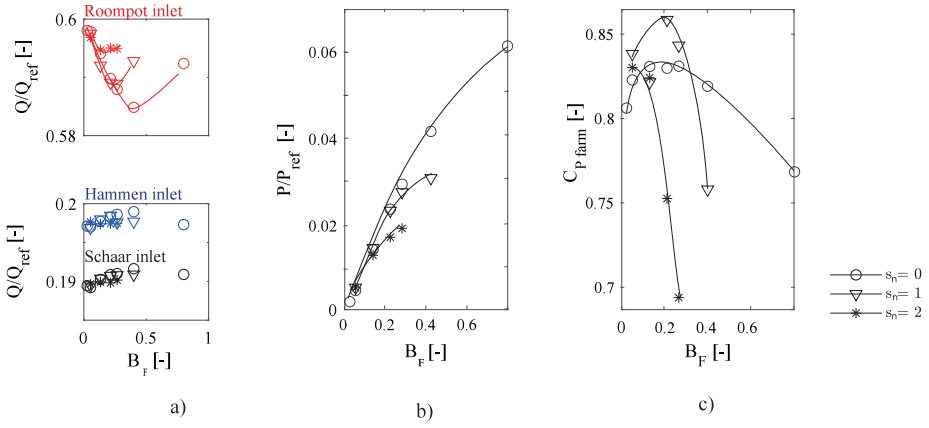

Fig. 10. Scenarios for turbine placement in the Roompot inlet: computed tidal volume and turbine performance characteristics versus global blockage (B_F); tidal volume (V) passing the respective inlets (Roompot, Schaar and Hammen), normalized by the tidal volume (V_{ref}) in the reference scenario (a), total power output of turbines (P) normalized by a theoretical maximum given by $P_{\text{ref}} = \rho g \int \Delta H Q \, dt$, where ΔH is the available water level head and Q the corresponding discharge through the barrage in the reference scenario (b), time-averaged power coefficient of the installed turbines ($C_{P,\text{farm}} = P/(\rho g \int \Delta H Q_{\text{turbine}} dt)$, where ΔH is the water level head available at the barrage gates and Q_{turbine} the corresponding discharge through the installed turbine area in the gates.) (c); all panels present data for one model day, interpolation splines are added as visual aid only.

where arrays of turbines also occupy the gates nearest to the shore lines. This involves a more uniform distribution of the resistance over the barrage width, which reduces the lateral velocity gradient and the associated expansion losses in the wake flow. In any case, the loss of tidal volume in the Roompot is almost completely compensated by a corresponding increase in the other two inlets, Hammen and Schaar, the overall impact of the turbines on the tidal exchange being less than 1%.

Fig. 10b presents the overall power output of the turbines for the considered scenarios normalized with the total power available in the flow passing the inlet. Generally, the power output increases with the number of turbines. For a given global blockage, the output is highest when turbines are placed in neighbouring gates ($s_n = 0$) and lowest when arrays are separated by two empty gates ($s_n = 2$). The latter is the result of the increased inter-array bypass flow when the array blockage decreases. At the same time, the marginal output decreases when installing more turbines, moreover when the global blockage is large. This is attributed to the deployment of less effective arrays in the nearshore gates of the barrage where the depth and flow velocities are relatively small.

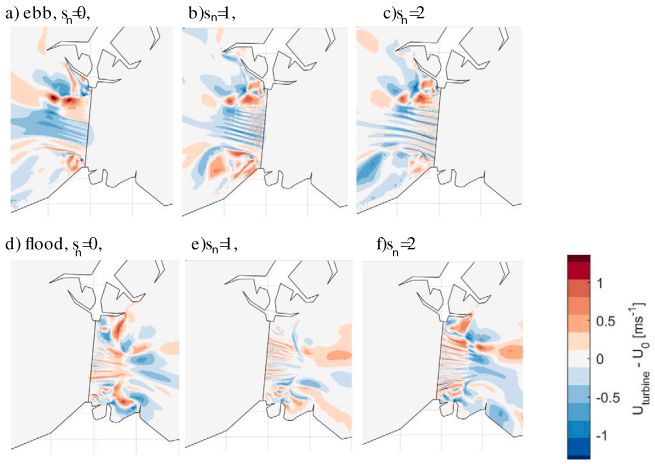

Fig. 11. Ambient flow effects: velocity deviation in the southern channel inlet (Roompot), relative to the reference scenario, for scenarios with ten arrays of turbines; upper panels: maximum ebb flow for $s_n = 0$ (a), $s_n = 1$ (b) and $s_n = 2$ (c); lower panels: maximum flood flow for $s_n = 0$ (d), $s_n = 1$ (e) and $s_n = 2$ (f).

Fig. 10c displays the power coefficient, which is a widely used variable to express the efficiency of turbines for harvesting energy from the flow. Interestingly, the scenarios with an inter-array spacing of one gate ($s_n = 1, B_A = 0.5$) have the highest power coefficient, which peaks at 0.86. This confirms the analytical prediction in [7], who found a peak value of 0.865 for an optimal array blockage of 0.4. For $s_n = 1$, the power coefficient decreases to about 0.75 if the global blockage exceeds 0.3, which is equivalent to more than ten gates being filled with turbines. As similar decline occurs for both the other inter-array spacings ($s_n = 0, s_n = 2$), albeit for a different total number of turbines. The inclusion of gates near the sides of the tidal inlet channel when the number of turbines approaches its maximum limit is the most important factor explaining this effect.

3.4.3. Turbine scenarios: ambient flow effects

The effects of the turbines on the ambient flow patterns in the Roompot tidal inlet are discussed by considering two moments during ebb and flood, respectively, for which the head difference over the barrage and the corresponding flow velocities are maximum. As an example, Fig. 11 shows spatial patterns of the flow velocity deviation, relative to the reference situation, for all scenarios with 10 gates being filled with turbines. This number is chosen since it translates to a global blockage that is close to the theoretical optimum for energy extraction [7].

Downstream of the barrage, the flow velocity decreases *behind* the gates with turbines (the wake), and increases *between* gates with turbines (the bypass). A similar pattern can be recognized at the scale of the tidal farm as a whole, where downstream of the farm the flow is generally decelerating, while in the large-scale bypass around the farm the flow is mostly accelerating. The farm thus redistributes the discharge in the tidal channel, which is characterized by a reduction of the flow contraction behind the barrage.

Upstream of the barrage, the ebb flow decelerates towards the tidal farm over a rather uniform zone, while during flood the deceleration occurs over confined areas just upstream of individual turbine arrays. This indicates that during ebb the gate-gate interaction is governed by the global blockage while during flood the array blockage is more prominent in this respect. This stems from the deployment of the turbines on the landward side of the barrage gates, which implies a larger added resistance during ebb, and a more pronounced effect on the flow fields, compared to the flood situation. The latter is a consequence of the flow resistance calculated in the sub-grid model, using different head-discharge relations for ebb and flood, respectively. In fact, the adapted internal boundary approach does not produce a numerical boundary layer in the flow upstream of the turbine [18]. For the same reason (results not shown here), a larger impact occurs when either more gates are filled with turbines (increasing the global blockage), or when turbine arrays are placed closer to each other (decreasing the array blockage), moreover so during ebb.

At basin scale, the influence of the turbines on the flow pattern extends beyond the Roompot tidal inlet, by means of their added resistance. The latter depends on the global blockage and the position of the turbines with respect to the flow direction (i.e., ebb or flood). The added resistance increases the head difference over the barrage, compared to the reference situation, and causes a small time lag of the tidal water level variation in the entire basin. This increases the discharge in the two northern inlets Hammen and Schaar, where the additional resistance is absent, which almost compensates for the decreased discharge in the Roompot inlet.

The above analysis reveals a clear relation between the added resistance and the redistribution of the flow over the barrage across a range of scales, from a single array of turbines to one tidal inlet and even the entire basin entrance. This may be utilized to manipulate the tidal jet, mitigating its scouring potential that presently causes ongoing erosion downstream of the barrage.

4. Discussion

The discussion will first address the application range of the proposed model and its further development steps. Thereafter, different turbine configurations and their trade offs and compromises are discussed.

4.1. Model application range

This article proposes a model for optimizing the configuration of turbine fences over a barrage with parallel gates, in order to harvest energy from the flow while respecting environmental constraints of the hinter-lying basin. The model can be applied during both the start-up and the realization of a tidal energy project. In both phases, changes in hydrodynamic patterns and energy yield need to be explored for alternative turbine configurations, as this is key to balance multiple criteria regarding harvesting energy and sustaining barrage integrity within environmental constraints.

We are not alone in pursuing such a modelling tool; some other numerical models have been proposed in literature for simulating the performance of free stream turbines in different (farm) configurations [14,29], or for alternative barrage designs [9]. A key novelty of our method is that it blends former approaches, providing a simulation tool for a hybrid of these technologies, which is validated against

elaborate and unique sets of both experimental and full-scale turbine data capturing the turbine-barrage interaction. The latter suggests the use of an unstructured mesh for the shallow-water flow model in order to resolve the interaction of the turbines with a barrage as well as with a complex basin bathymetry, over a wide range of scales, an approach that is also favoured in [9]. In addition, we show how to apply the model to a unique and thoroughly monitored field case.

In the analysis of this pilot, it was suggested that certain turbine configurations can solve local issues in the hydrodynamics by using a dedicated turbine-configuration. In particular, the lateral velocity profile in the adjacent tidal channel can be manipulated, decreasing the contraction of the tidal jets, which reduces the scouring potential of the flow downstream of the barrage.

As a first step, the present work intended to investigate the flow processes in the basin driving the turbines, using fixed turbine — and configuration settings. For applying the developed tool to future tidal energy projects, a useful extension of the model would be an automatic optimization of these settings with regard to the underlying project goals. For our target application of a hybrid between tidal stream and barrage, different thresholds or weights would be needed, reflecting the project criteria, in order to make an automatic optimization feasible.

There are some assumptions in the sub-grid model that may lead to deviations from the observations. In particular, the neglect of the yawing phenomenon of the turbine (i.e., power reduction under angled inflow [30]), the exclusion of a correction for high velocities (when blades operate in deep stall), and the neglect of Froude-number dependent blockage (increasing the blockage effect for high flow velocities [16]). However, in the considered case of the Eastern Scheldt these conditions hardly occur, justifying the above simplifications. Other assumptions made in the sub-grid model concern the linear integration of forces over the rotor swept area, and the neglect of rotational effects of the wake and 3D flow effects at the blade tip. These are only of minor importance because of the (large) spatial scales of interest of this study.

4.2. Trade-offs and compromises of farm configurations

The optimal configuration of turbines in a barrage is not simply dictated by a numerical result only. In particular, the configuration yielding a maximum energy extraction, when all gates are filled, may involve compromises regarding the structural integrity of a barrage and the ecological impact, the latter being expressed as a reduction of the tidal volume. All trade-offs and compromises have to be put into perspective before adopting a particular alternative. We therefore reconsider the implications for the Eastern Scheldt case, followed by a short discussion of other tidal farm locations, arriving finally at the broader implementation of the EU targets.

Our analysis shows that, accepting a change of the tidal volume of at most 1 percent of the reference situation, room for at least 10 gates with turbines is present. They harvest most energy from the flow (highest power output per turbine area, and highest degree of gate-gate enhancement) when configured directly neighbouring each other in the centre of the inlet, where the flow velocity is highest. An additional advantage of this choice, regarding the structural integrity of the barrage, is that the contraction of the tidal jet in the inlet is suppressed by this configuration. The latter may decrease the scour potential of the flow at either side of the barrage, as was discussed in Section 3.1. Besides, the flow asymmetry enforced with a turbine deployment in only one of the three tidal inlets, may induce more sediment transport into the basin than a more symmetric arrangement where turbines are spread evenly over the three inlets [31]. This is considered favourable for sustaining the biodiverse tidal flats in the area, as discussed in Section 3.1.

In other turbine–barrage projects around the world, finding the right balance between environmental (flow) effects and turbine energy yield is also a prerequisite. For example, in the Larantuka Strait, Indonesia, where a so-called tidal bridge is planned, both energy yield and the far field flow effects are crucial for its realization [32]. In this respect it is noteworthy that the presented research shows that the far-field flow effects of turbines inside barrages are relatively small. In particular, the added resistance of turbines in an open barrage appears to be lower than estimated before [31,33], rendering the estimates less conservative. This enables projects to combine a relatively high energy yield (trade-off) with a limited environmental impact, provided the proper choices are made. The proposed model can help in finding this balance.

5. Conclusion

The twofold aim of the research described in this paper was, first, to develop an accurate and efficient model to study an optimal configuration of turbine fences in a barrage, and second, to apply it to a realistic tidal site for investigating the energy yield of a tidal farm, and its impact on the tidal volume and flow distribution. This hinges on the idea that the turbine-barrage interaction with the adjacent basin can be modelled using a head-discharge relation (to incorporate turbine-barrage interaction) combined with sufficient resolution (to incorporate turbine-turbine interaction on account of their bypass flows). In order to achieve the first aim, the relevant effects of barrage-mounted turbine fences were parameterized, in terms of head-discharge relations, for an efficient numerical implementation. This parameterization was then coupled to a shallow water flow model which is based on the finite element method. The turbines are implemented by means of interior boundaries along which the head-discharge relations for barrage-mounted turbines are prescribed. The latter are derived from an analytical model which was validated using field and experimental data. Novel aspects addressed by this study are: the modelling of turbine fences with barrages, including details of the near-field, and its validation against elaborate data obtained specifically for this type of tidal power. The latter originating from commercial-scale operating turbines in a barrage (shared publicly by the turbine company), and a corresponding scaled experimental turbine (with a relatively large scale factor).

To achieve the second aim, the model is applied to a thoroughly monitored tidal energy pilot project in the Eastern Scheldt basin. The analysis shows that smart placing of the turbines can lead to a 50% increase of the harvested power for the same number of turbines. For a scenario with ten gates being filled with turbines, summing up to 50 turbines, the tidal volume decreases with only 1.5%. A minimal tidal volume change is crucial at this location as the tidal prism accounts for the transport of nutrients and sediments to the biodiverse tidal flats in the hinter-lying basin. The results furthermore show the potential use of turbines to manipulate the tidal jet issued from the barrier, in favour of coastal protection. In particular, this may reduce the ongoing scour of the tidal channels near the barrage. For the Eastern Scheldt, the above considerations result in an optimum with around 10 gates being filled with turbines — situated in the centre of the barrage.

In essence, choosing an optimum tidal farm configuration is far more complex than achieving the largest power output only. The developed modelling tool can be used to understand how complex EU ambitions on coastal protection and energy generation within environmental constraints can be combined in a tidal energy project.

CRediT authorship contribution statement

M.C. Verbeek: Conceptualization, Methodology, Writing – original draft, Visualization, Investigation, Validation. **H. Talstra:** Software, Writing – original draft. **R.J. Labeur:** Writing – review & editing, Funding acquisition, Conceptualization. **W.S.J. Uijttewaal:** Supervision.

Declaration of competing interest

The authors declare that they have no known competing financial interests or personal relationships that could have appeared to influence the work reported in this paper.

Acknowledgements

This work is financed by the Netherlands Organisation for Scientific Research (NWO) within the research programme The New Delta (project number 869.15.008). We are grateful to Svašek Hydraulics for making their FINEL software available, the use of their computer cluster and the assistance in programming. Tocardo is thanked for sharing data on their tidal power station. The European Regional Development Fund (ERDF) OP-Zuid 2014–2020 programme is acknowledged for their financial support.

Appendix A. Sub-grid turbine model

A.1. Turbine parameterization

The turbine parameterization relates the local water level difference over the turbine-weir configuration to the following output,

- the discharge q (per unit width) through a barrage gate with or without turbines (discharge relation),
- the net thrust force T on the turbines,
- the power yield P of the turbines.[2]

The parameterization is based on an analytical model proposed in [4] which was validated experimentally in [5]. The corresponding discharge relations have been adapted to include the cases of a weir without turbines and turbines on a flat bed as well. The resulting discharge relation takes the following general form,

$$q = d_c u_c = d_c \sqrt{\frac{2g\Delta h}{f}} \tag{A.1}$$

in which d_c and u_c are, respectively, the depth and the depth-averaged flow velocity at the weir crest, g is the gravitational acceleration, Δh is the local head difference over the turbine/weir, and f is a dimensionless head loss coefficient.

The expression for f is specific to the chosen turbine-weir configuration. Four different cases are distinguished,

1. turbine on a flat bed (no weir)
2. turbine upstream of a weir
3. turbine downstream of a weir
4. weir only (no or idle turbine)

These cases are characterized by two dimensionless parameters. The relative weir height a is defined as the height of the weir relative to the water depth near the weir, as follows,

$$a = \frac{d_1 - d_c}{d_c} = \frac{d_7 - d_c}{d_c} \tag{A.2}$$

in which d_1 is the water depth upstream of the weir, assumed equal to the downstream water depth d_7, see Fig. A.12. The so-called inverse blockage ratio R is defined as the (reciprocal) fraction of the flow cross-section at the weir blocked by the turbines, as follows,

$$R = \frac{1}{B_L} = \frac{d_c}{A_D} \tag{A.3}$$

in which D is the turbine diameter, s_L is the intra-turbine spacing, and A_D is the rotor swept area of the turbine per unit width, see also Eq. (2). Note that for a turbine on a flat bed a equals zero, while for a weir without turbine R tends to infinity.

The flow distribution over the weir and turbines is schematized by means of two streamtubes (see Fig. A.12), a stream tube passing the turbine rotor, indicated D, and a stream tube covering the flow bypass, indicated B. In addition, we discern a flow recirculation zone downstream of the weir. Furthermore, the schematization assumes a uniform water level over the weir-turbine, for which a weighted average of the upstream and downstream water levels is used [23]. Thus, the water level difference Δh only acts in a dynamic way, driving the flow, while its effect on the flow kinematics (i.e., flow cross-section) is ignored. This is allowed if the water level difference Δh is negligible relative to the local water depth.

For both streamtubes one-dimensional balances of mass, momentum and energy apply. These balances are expressed in terms of dimensionless velocity coefficients α_n (streamtube D) and β_n (streamtube B), where n is an index referring to the corresponding station (see Fig. A.12). In particular, the coefficient α_5 (velocity in the turbine wake relative to u_c) is treated as an independent input parameter, representing the actual operational settings of the turbine system. Assuming a constant discharge (quasi-steady flow) and a hydrostatic pressure in every station but 3 and 4, the balances are coupled which results in a set of equations that, given a, R and α_5, can be solved to yield the flow and pressure distributions along both streamtubes. The algebra is lengthy, and the complete derivation and solution are provided in the supplementary material [23]. The resulting expressions for the head-loss coefficient are given by,

$$\begin{aligned}
&\text{turbine on a flat bed (no weir) [11]} && f = \frac{\beta_5^2 - \alpha_5^2}{R} \\
&\text{turbine upstream of a weir} && f = \frac{\beta_5^2 - \alpha_5^2}{R} + 2\left(\frac{a}{1+a}\right)^2 \\
& && \quad + \frac{a}{2+a}\left[\left(\frac{1}{1+a}\right)^2 - \beta_5^2\right] \\
&\text{turbine downstream of a weir} && f = \frac{\beta_5^2 - \alpha_5^2}{R(1+a)} + \left(\frac{a}{1+a}\right)^2 \\
&\text{weir only, no turbine [22]} && f = \left(\frac{a}{1+a}\right)^2
\end{aligned} \tag{A.4}$$

in which the coefficient β_5 (velocity in the wake bypass relative to u_c) is implicitly given by,

$$Ry\left(\beta_5^2 - 1\right) - \left(\beta_5^2 - \alpha_5^2\right) + 2R\left(1 - \beta_5\right)\left(1 - \alpha_5\right) = 0 \tag{A.5}$$

where y is a flow expansion factor defined by $(2+2a)/(2+a)$ for an upstream turbine, and by $1 + a$ otherwise. After solving for β_5, the coefficient α_3 (velocity at the rotor plane relative to u_c, or *induction*), follows from,

$$\alpha_3 = \frac{R\left(1 - \beta_5\right)}{1 - \beta_5/\alpha_5} \tag{A.6}$$

To complete Eq. (A.1), the water level difference Δh is obtained from the shallow water flow model. The resulting specific discharge q is fed back into the flow model by imposing it as an interior boundary condition.

The following general formula holds for the net axial force T on the turbines (thrust force) per unit width,

$$T = \frac{1}{2}\rho u_c^2 A_D\left(\beta_5^2 - \alpha_5^2\right) = \frac{1}{2}\rho u_c^2 A_D C_T \tag{A.7}$$

in which $C_T = \beta_5^2 - \alpha_5^2$ is the dimensionless thrust coefficient. Multiplying the thrust force by the local flow velocity $\alpha_3 u_c$ at the turbine disk returns the corresponding power yield P per unit width,

$$P = \frac{1}{2}\rho u_c^3 A_D \alpha_3\left(\beta_5^2 - \alpha_5^2\right) = \frac{1}{2}\rho u_c^3 A_D C_P \tag{A.8}$$

in which $C_P = \alpha_3 C_T = \alpha_3\left(\beta_5^2 - \alpha_5^2\right)$ is the dimensionless power coefficient. We recall that P must be scaled by the electrical efficiency η to obtain the effective power yield ηP.

[2] The gross amount of energy extracted from the flow will always be reduced by some efficiency factor $\eta < 1$, to obtain the effective net electrical power yield. However, this efficiency factor has no feedback on the local hydrodynamics and is therefore omitted from the analyses.

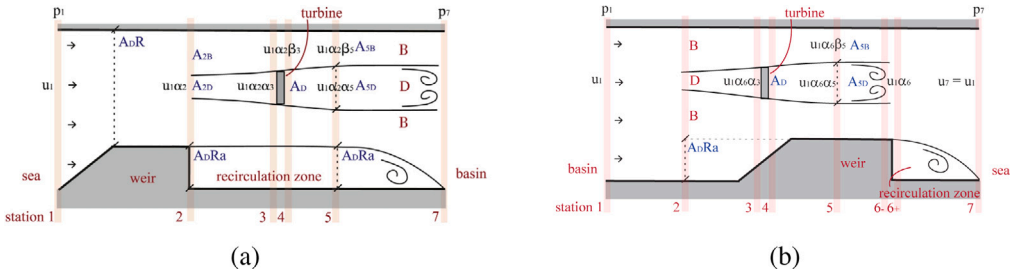

Fig. A.12. Schematization of the flow passing the weir and turbine: turbine downstream of weir as during flood (a), turbine upstream of weir as during ebb (b).

Appendix B. Shallow water flow

The shallow-water equations are valid when the horizontal dimensions of the considered flow problem exceed, by far, the water depth. In such case the vertical pressure distribution can be assumed hydrostatic while variations of the flow velocity over depth are presumably small. This allows vertical integration of the basic balance equations for fluid motion, expressing these in terms of vertically averaged quantities. Although not strictly necessary, the atmospheric pressure and water density are assumed to be uniform, for simplicity.

We first consider the depth-integrated continuity equation describing the mass balance in a horizontal flow. For a uniform density, this reduces to a volume balance equation, which reads as follows

$$\frac{\partial d}{\partial t} + \nabla \cdot (d\bar{u}) = 0, \tag{B.1}$$

where d is the water depth, $\bar{u}$ is the depth-averaged flow velocity vector, and ∇ denotes the horizontal gradient operator.

Second, the depth-integrated momentum balance equations describe the balance of forces acting on a fluid particle. In the shallow-water approximation this concerns the pressure gradient, assumed vertically uniform, the transfer of horizontal momentum by mean advection and turbulence, (wind) shear stresses at the sea surface, and bed friction. These equations are stated as follows

$$d\left(\frac{\partial \bar{u}}{\partial t} + \bar{u} \cdot \nabla \bar{u}\right) + gd\,\nabla h + \nabla \cdot (d\bar{\bar{\tau}}_t) = \bar{\tau}_w - \bar{\tau}_b \tag{B.2}$$

where h is the water level, g is gravitation, $\bar{\bar{\tau}}_t$ is the turbulence stress tensor, $\bar{\tau}_w$ is the wind shear stress at the sea surface, and $\bar{\tau}_b$ is the bed shear stress opposed to the flow direction (stresses are normalized with the water density). Eq. (B.2) is the so-called acceleration form of the momentum equations; other equivalent forms can be derived depending on the primary variables that are being considered.

Appendix C. Supplementary data

Supplementary material related to this article can be found online at https://doi.org/10.1016/j.renene.2023.119929.

References

[1] EU, The European Green Deal, Tech. Rep. 640, European Commission, 2019.

[2] A.G.L. Borthwick, Marine renewable energy seascape, Engineering 2 (1) (2016) 69–78, http://dx.doi.org/10.1016/J.ENG.2016.01.011.

[3] M. Leopold, M.e. Scholl, Monitoring getijdenturbines oosterscheldekering jaarrapportage 2018, (Tech. Rep. C010/19) Wageningen Marine Research Den Helder, Wageningen UR (University and Research centre), 2019, pp. 1–58, http://dx.doi.org/10.18174/470409.

[4] M. Verbeek, R. Labeur, W. Uijttewaal, The performance of a weir-mounted tidal turbine: Field observations and theoretical modelling, Renew. Energy 153 (2020) 601–614, http://dx.doi.org/10.1016/j.renene.2020.02.005, URL http://www.sciencedirect.com/science/article/pii/S0960148120301853.

[5] M.C. Verbeek, R.J. Labeur, W.S.J. Uijttewaal, The performance of a weir-mounted turbine - experimental investigation, Renew. Energy 168 (2021) 64–75, http://dx.doi.org/10.1016/j.renene.2020.12.013.

[6] T. Nishino, R.H.J. Willden, Two-scale dynamics of flow past a partial cross-stream array of tidal turbines, J. Fluid Mech. 730 (2013) 220–244, http://dx.doi.org/10.1017/jfm.2013.340.

[7] S. Cooke, R. Willden, B. Byrne, The potential of cross-stream aligned sub-arrays to increase tidal turbine efficiency, Renew. Energy 97 (Supplement C) (2016) 284–292, http://dx.doi.org/10.1016/j.renene.2016.05.087, URL http://www.sciencedirect.com/science/article/pii/S0960148116304979.

[8] S. Draper, Modelling tidal energy extraction in a depth-averaged coastal domain, IET Renew. Power Gener. 4 (2010) 545–554, http://dx.doi.org/10.1049/iet-rpg.2009.0196, (9).

[9] A. Angeloudis, R.A. Falconer, S. Bray, R. Ahmadian, Representation and operation of tidal energy impoundments in a coastal hydrodynamic model, Renew. Energy 99 (2016) 1103–1115, http://dx.doi.org/10.1016/j.renene.2016.08.004, URL https://www.sciencedirect.com/science/article/pii/S0960148116307042.

[10] T.A.A. Adcock, S. Draper, G.T. Houlsby, A.G.L. Borthwick, S. Serhadlıoğlu, The available power from tidal stream turbines in the pentland firth, Proc. R. Soc. A 469 (2157) (2013) 20130072, http://dx.doi.org/10.1098/rspa.2013.0072.

[11] C. Garrett, P. Cummins, The efficiency of a turbine in a tidal channel, J. Fluid Mech. 588 (2007) 243–251, http://dx.doi.org/10.1017/S0022112007007781.

[12] Y.B. Broekema, Horizontal shear flows over a streamwise varying bathymetry (Ph.D. thesis), Delft University of Technology, 2020, http://dx.doi.org/10.4233/uuid:016ee80a-fba2-4534-a578-94e7b35022a9.

[13] R. Vennell, S. Funke, S. Draper, C. Stevens, T. Divett, Designing large arrays of tidal turbines: A synthesis and review, Renew. Sustain. Energy Rev. 41 (2015) 454–472, http://dx.doi.org/10.1016/j.rser.2014.08.022.

[14] T. Nishino, R.H. Willden, Effects of 3-D channel blockage and turbulent wake mixing on the limit of power extraction by tidal turbines, Int. J. Heat Fluid Flow 37 (2012) 123–135, http://dx.doi.org/10.1016/j.ijheatfluidflow.2012.05.002.

[15] A. Betz, Das maximum der theoretisch möglichen ausnützung des windes durch windmotoren, Z. Gesamte Turbin. Heft 26 (1920) Seiten 307 bis 309.

[16] J.I. Whelan, J.M.R. Graham, J. Peiro, A free-surface and blockage correction for tidal turbines, J. Fluid Mech. 624 (2009) 281–291, http://dx.doi.org/10.1017/S0022112009005916.

[17] J.A. Battjes, R.J. Labeur, Unsteady Flow in Open Channels, Cambridge University Press, 2017, http://dx.doi.org/10.1017/9781316576878.

[18] R. Labeur, Finite element modelling of transport and non-hydrostatic flow in environmental fluid mechanics, TU Delft Repos. (2009) 1–235, https://resolver.tudelft.nl/uuid:7b2d7144-4ea8-4bba-9a05-14ec761b43c3.

[19] R. Labeur, G. Wells, Interface stabilised finite element method for moving domains and free surface flows, Comput. Methods Appl. Mech. Engrg. 198 (5–8) (2009) 615–630, http://dx.doi.org/10.1016/j.cma.2008.09.014.

[20] R. Labeur, G. Wells, Energy stable and momentum conservative interface stabilised finite element method for the incompressible Navier-Stokes equations, SIAM J. Sci. Comput. 34 (2) (2012) A889–A913.

[21] Y. Steenman, Numerical modelling of shallow jet flows - Case study of Waterdunen (Master's thesis), Delft University of Technology, Faculty of Civil Engineering and Geosciences, 2020, URL http://resolver.tudelft.nl/uuid:6117649e-2aa4-4f45-8a4b-f35c9ec22623.

[22] H. Talstra, B. Van Leeuwen, L. De Wit, Improving accuracy of weir/groyne discharge formulations for highly sub-critical (submerged) conditions, 2019, Land of Rivers, NCR Days 2019 Utrecht, (2019–43), 83–84.

[23] M. Verbeek, H. Talstra, R. Labeur, W. Uijttewaal, Supporting material, 2022, https://link.to.supplementary.material.

[24] H. Talstra, Large-scale turbulence structures in shallow separating flows (Ph.D. thesis), 2011, URL http://resolver.tudelft.nl/uuid:922e297b-19b9-4399-808d-23e837401a52,

[25] Y.B. Broekema, R.J. Labeur, W.S.J. Uijttewaal, Observations and analysis of the horizontal structure of a tidal jet at deep scour holes, J. Geophys. Res. Earth Surf. 123 (12) (2018) 3162–3189, http://dx.doi.org/10.1029/2018JF004754, arXiv:https://agupubs.onlinelibrary.wiley.com/doi/pdf/10.1029/2018JF004754.

[26] T. Louters, J.H. van den Berg, J.P.M. Mulder, Geomorphological changes of the oosterschelde tidal system during and after the implementation of the delta project, J. Coast. Res. 14 (1998) 1134–1151.

[27] B. van Leeuwen, Validatie van het oosterscheldemodel, sophiastrand, Svasek Hydraul. (2016) 1–3.

[28] A. Valle-Levinson, X. Guo, Asymmetries in tidal flow over a seto inland sea scour pit, J. Mar. Res. 67 (2009) 619–635, http://dx.doi.org/10.1357/002224009791218850.

[29] S. Funke, P. Farrell, M. Piggott, Tidal turbine array optimisation using the adjoint approach, Renew. Energy 63 (2014) 658–673, http://dx.doi.org/10.1016/j.renene.2013.09.031, URL https://www.sciencedirect.com/science/article/pii/S0960148113004989.

[30] A. Bahaj, W. Batten, G. McCann, Experimental verifications of numerical predictions for the hydrodynamic performance of horizontal axis marine current turbines, Renew. Energy 32 (15) (2007) 2479–2490, http://dx.doi.org/10.1016/j.renene.2007.10.001.

[31] V.M. Gatto, R.J. Labeur, B.C. van Prooijen, Z.B. Wang, Rapid assessment of (small) morphological impacts in intertidal systems: methodology and application to tidal energy, Coast. Eng. (2022, submitted).

[32] A.M. Firdaus, G.T. Houlsby, T.A.A. Adcock, Tidal energy resource in larantuka strait, Indonesia, Proc. Inst. Civil Eng. Energy 173 (2) (2020) 81–92, http://dx.doi.org/10.1680/jener.19.00042.

[33] P. Ouro, T. Stoesser, Impact of environmental turbulence on the performance and loadings of a tidal stream turbine, Flow Turbul. Combust. 102 (2019) http://dx.doi.org/10.1007/s10494-018-9975-6.